RSC Advances

ROYAL SOCIETY OF CHEMISTRY

www.rsc.org/advances

Multifunctional Zn(II)/Cd(II) Metal Complexes for Tunable Luminescence Properties and High Efficient Dye-Sensitized Solar Cells

Song Gao,[a] Rui Qing Fan,*[a] Xin Ming Wang,[a] Liang Sheng Qiang,[a] Li Guo Wei,[a] Ping Wang,[a] Yu Lin Yang,*[a] Yu Lei Wang,[b] Tian Zhu Luan[c]

[a] *Department of Chemistry, Harbin Institute of Technology, Harbin 150001, P. R. China*

[b] *National Key Laboratory of Science and Technology on Tunable Laser, Harbin Institute of Technology, Harbin 150080, P. R. China*

[c] *The First Affiliated Hospital of Harbin Medical University, Harbin, 150001, P. R. China*

To whom the proofs and correspondence should be sent.

Professor Rui-Qing Fan

Department of Chemistry

Harbin Institute of Technology Harbin 150001, P. R. China

Fax: +86-451-86413710

E-mail: fanruiqing@hit.edu.cn and ylyang@hit.edu.cn

We design two novel d^{10} metal complexes $[Zn(3\text{-qlc})_2]_n$ (**Zn1**), $[Cd(3\text{-qlc})_2]_n$ (**Cd1**) (3-Hqlc = quinoline-3-carboxylic acid), which display alike 2D layer structures, and further form 3D 6-connected primitive cubic (**pcu**) network topology *via* $\pi\cdots\pi$ stacking interactions with the point symbol of $\{4^{12}.6^3\}$. Complexes **Zn1** and **Cd1** exhibit tunable luminescence and photovoltaic properties as new type of multifunctional materials. **Zn1** and **Cd1** show tunable luminescence from blue to green by varying the temperature in the solid state. What's more, both of them exhibit excellent aggregation-induced emission (AIE) properties in DMSO/water mixtures. Encouraged by the UV-visible absorption in ethanol solution result, **Zn1** and **Cd1** can be considered as co-sensitizers in combination with N719 to investigate their effect on enhancing the dye-sensitized solar cells (DSSCs) performance. **Zn1** and **Cd1** could overcome the deficiency of ruthenium complex N719 absorption in the region of ultraviolet and blue-violet, offsetting competitive visible light absorption of I_3^- and reducing charge recombination of injected electron. After co-sensitized with **Zn1** and **Cd1**, the device co-sensitized by **Zn1**/N719 and **Cd1**/N719 yield an overall efficiency of 7.75% and 7.70%, which are 44.59% and 43.66% higher than that of the device sensitized only by N719 (5.36%).

Introduction

The past two decades have witnessed the rapid development of metal coordination complexes (MCCs) due to their fantastic structures and wide potential applications.[1-3] Recently, the design of MCCs with excellent luminescence and photovoltaic properties has attracted increasing attention in pursuit of multifunctional materials.[4-6] The main bottleneck in improving the efficiency of photovoltaic energy conversion lies in the spectral mismatch between the energy distribution of photons in the incident solar spectrum and the band-gap of a semiconductor material.[7,8] Multiple sensitizers taking advantage of MCCs as co-sensitization would appear to be more achievable in improving the absorption ability of solar cell.[9,10] As typical representative of DSSC sensitization, N719 shows low utilization in ultraviolet and blue-violet light region, and the research about light utilization in high energy blue-violet light region has been little reported.[11] Some MCCs as co-sensitizer or co-adsorbent in DSSCs not only compensate the absorption spectra but also overcome the competitive light absorption by I^-/I_3^- and reduce charge recombination, which will enhance the DSSCs performance by co-sensitization.[12,13] Consequently, the

reasonable design of MCCs as co-sensitizers for high-efficiency DSSC is still a big challenge and of great importance.

The key to design MCCs materials is the matching of organic ligand and central metal ion which can provide the platform to generate ultraviolet absorption and luminescence.[14-17] Quinoline-3-carboxylic acid (3-Hqlc) as N-heterocyclic carboxylate ligand has attracted increasing attention in the preparation of interesting polymeric frameworks for their outstanding features of versatile coordination fashions.[18] It has a relatively large π-conjugated system in the quinoline ring, which not only contribute to the desirable ultraviolet absorption and luminescence properties resulting from the interaction between 3-qlc⁻ anions and metal ions, but also easily assemble into high dimensional supramolecular network *via* C–H··· π / π···π stacking interactions between two adjacent aromatic rings as well as hydrogen bonding interactions, adding additional stability to these structures.[19]

The enormous variability of available ligand–metal combinations opens the possibility of creating luminescence "by design". The d^{10} metal complexes have gained intensive attention because of relatively low-cost, intriguing structures and adequate electron transport, which are advantageous to enhance the luminescence efficiency.[20,21] On the basis of the above considerations, we aim to synthesize d^{10} metal complexes with strong absorption in ultraviolet and blue-violet light region, in order to replace noble metal complexes (metal osmium (II), platinum (II) and ruthenium (II) MCCs doped semiconductors) as co-sensitizers.[22-24]

Herein, we report the design and synthesis of two new d^{10} metal complexes, $[Zn(3\text{-}qlc)_2]_n$ (**Zn1**), $[Cd(3\text{-}qlc)_2]_n$ (**Cd1**). **Zn1** and **Cd1** exhibit luminescence with emission maxima containing blue and green at 298 K and 77 K, respectively, in the solid state. **Zn1** and **Cd1** display excellent aggregation-induced emission (AIE) properties in the solid state, which show weak emission in DMSO (good solvent) but are brightly luminescent by the addition of water (poor solvent) due to aggregation. Therefore, **Zn1** and **Cd1** offer great opportunities for the design of luminescence solid films materials.[25,26] In addition, as a result of their strong absorption in the wavelength range 300–400 nm, **Zn1** and **Cd1** are employed as co-sensitizers with the well-known ruthenium N719 dye based solar cell, and the co-sensitized devices exhibited enhancements of photovoltaic performance. It showed that the absorption spectra of complexes **Zn1** and **Cd1** could compensate that of N719 absorption in the region of ultraviolet and blue-violet, the light harvesting was enhanced. The power conversion

efficiency of N719 sensitized DSSC is enhanced by 44.59% and 43.66% after co-sensitized with **Zn1** and **Cd1** than that for DSSCs using single N719 (5.36%), which indicating that **Zn1** or **Cd1** is a promising candidate as co-sensitizer for high efficiency DSSCs and does help to improve the devices performance. Hence, this strategy may provide interesting insight into the development of high-performance DSSCs devices.

Experimental Section

General characterization

All materials and reagents were commercially available and used without further purification. IR spectra were obtained from KBr pellets using a Nicolet Avatar-360 infrared spectrometer in the 4000-400 cm^{-1} region. Elemental analyses (C H and N) were performed on a Perkin-Elmer 240c element analyzer. The thermal analysis was performed on a ZRY-2P thermogravimetric analysis from 30°C to 700 °C with heating rate of 10 °C min^{-1} under a flow of air. UV-visible spectra were obtained using a Perkin-Elmer Lambda 20 spectrometer. Powder X-ray diffraction (PXRD) patterns were PANalytical, monochromated Cu Kα radiation 40 mA, 40 kV. The solid-state and solution luminescence analyses were carried out on an Edinburgh FLS920 fluorescence spectrometer in the range of 200–800 nm. An Edinburgh Xe900 400 W Xenon is lamp was used as exciting light source. The visible detector as well as the lifetime setup was red-sensitive photomultiplier (type r928). Low temperature analyses were carried out at 77 K with an Oxford Optistat DN^{TM} cryostat (with liquid nitrogen filling). Lifetime studies were performed using photon-counting system with a microsecond pulse lamp as the excitation source. Data were analyzed through the nonlinear least squares procedure in combination with an iterative convolution method. The emission decays were analyzed by the sum of exponential functions. The decay curve is well fitted into a double exponential function: $I = I_0 + A_1 \exp(-t/\tau_1) + A_2 \exp(-t/\tau_2)$, where I and I_0 are the luminescent intensities at time $t = t$ and $t = 0$, respectively, whereas τ_1 and τ_2 are defined as the luminescent lifetimes. The average lifetime was calculated according to the following equation: $\dfrac{\tau_1^2 A_1\% + \tau_2^2 A_2\%}{\tau_1 A_1\% + \tau_2 A_2\%}$. For the solid samples, the absolute quantum yields have been measured by integrating sphere. The cyclic voltammetry (CV) were measured with a electrochemical workstation (CHI660D, Chenhua, Shanghai) using a three-electrode cell with a Pt working

electrode, a Pt wire auxiliary electrode, and a saturated calomel reference electrode in saturated KCl solution. The supporting electrolyte was 0.1 M tetrabutylammonium hexafluorophosphate (TBAPF$_6$, Fluka, electrochemical grade) in ethanol as the solvent. Photocurrent-photovoltage (*I-V*) curves were recorded by Keithley model 2400 digital source meter using a mask with an aperture area of 0.16 cm^{-2}. The irradiance of AM1.5 global sunlight from a filtered 500 W xenon lamp light source was set at 100 mW cm^{-2} and was calibrated by a standard silicon solar cell. Based on *I-V* curve, the fill factor (*FF*) is defined as: $FF = (J_{max} \times V_{max})/(J_{sc} \times V_{oc})$, where J_{max} and V_{max} are the photocurrent density and photovoltage for maximum power output; J_{sc} and V_{oc} are the short-circuit photocurrent density and open-circuit photovoltage, respectively. The overall energy conversion efficiency η is defined as: $\eta = (FF \times J_{sc} \times V_{oc})/P_{in}$ where P_{in} is the power of the incident light. IPCE spectra were recorded with Monochromatic incident photon-to-electron conversion efficiency (IPCE) were measured on an EQE/IPCE spectral response system (Newport). Electrochemical impedance spectroscopy (EIS) was recorded by CHI660D Electrochemical Analyzer (Chenhua, China), and the measurements were taken over a frequency range of 0.1-100 kHz under standard global AM1.5 solar irradiation or in the dark by applying a forward bias equivalent to V_{oc}.

Fabrication of Devices

The FTO conducting glass (Fluorine-doped SnO$_2$, sheet resistance 15 Ω per square, transmission 90% in the visible) was purchased from NSG, Japan, and cleaned by a standard procedure. N719 [*cis*-bis(isothiocyanato)bis (2,2-bipyridyl-4,4-dicarboxylato)-ruthenium(II)bis-tetrabutylammonium] was purchased from Solaronix Company, Switzerland. Dye-sensitized solar cells were fabricated using the following procedure. The TiO$_2$ paste was cast onto the FTO substrate by the screen-printing method, followed by drying at 100 ºC for 5 min and this process was repeated for six times, then followed by sintering at 500 ºC for 15 min in air to obtain a transparent TiO$_2$ photoelectrode with the thickness of ca. 10 μm. The co-adsorbent electrodes were prepared by immersing the obtained mesoporous TiO$_2$ photoelectrode into 0.3 mM **Zn1** or **Cd1** solution in absolute ethanol for 2 h and washed with ethanol and dried with blower, then further immersing the electrodes in 0.3 mM N719 solution in absolute ethanol for 12 h, and then washed with ethanol and dried with blower again. The single N719 sensitized electrodes were prepared by only immersing TiO$_2$ photoelectrode into 0.3 mM N719 solution in absolute ethanol for 14

h. The electrolyte used in this work was 0.5 M LiI + 0.05 M I$_2$ + 0.1 M *tert*-butyl pyridine in a 1:1 (volume ratio) of acetonitrile-propylene carbonate. The platinum counter electrode was prepared by depositing H$_2$PtCl$_6$ paste onto the FTO glass substrates and then sintered at 450 ºC for 30 min. The cells were assembled by sandwiching the electrolyte between the dye-sensitized photoanode and the counter electrode and assembly was held together using mini-binder clips.

Synthesis of [Zn(3-qlc)$_2$]$_n$ (Zn1)

A mixture of Zn(NO$_3$)$_2$·6H$_2$O (59.5 mg, 0.2 mmol), 3-Hqlc (17.3 mg, 0.1 mmol) were dissolved in H$_2$O (5 mL). After stirring for 30 minutes in air, it was transferred into a 15 mL Teflon–lined stainless steel autoclave and heated at 165 °C for 6 days. Then slow cooling to room temperature, yellow block crystals of **Zn1** were obtained in 72% yield (based on Zn). Anal. Calcd for C$_{20}$H$_{12}$N$_2$O$_4$Zn (*Mr*: 409.71): C, 58.63; H, 2.95; N, 6.84%. Found: C, 58.60; H, 2.96; N, 6.85%. IR (KBr pellet, cm^{-1}, Fig. S1) for **Zn1**: 3438(br, s), 1617(vs), 1572(m), 1522(m), 1458(w), 1373(s), 1305(m), 1269(w), 1242(w), 1206(w), 1174(w), 1115(m), 1066(m), 961(m), 844(m), 781(m), 699(w), 659(m), 582(m), 532(w), 496(w).

Synthesis of [Cd(3-qlc)$_2$]$_n$ (Cd1)

Complex **Cd1** was obtained by the same hydrothermal procedure as that for preparation of **Zn1** except that the metal salt was replaced by Cd(NO$_3$)$_2$·4H$_2$O (61.6 mg, 0.2 mmol). After the reaction mixture was cooled down to room temperature, yellow platelet crystals of **Cd1** were collected with a yield of 68% (based on Cd). Anal. Calcd for C$_{20}$H$_{12}$N$_2$O$_4$Cd (*Mr*: 456.73): C, 52.60; H, 2.65; N, 6.13%. Found: C, 52.63; H, 2.64; N, 6.12%. IR (KBr pellet, cm^{-1}, Fig. S1) for **Cd1**: 3442 (br, s), 1621(vs), 1580(m), 1549(m), 1504(m), 1468(s), 1409(vs), 1386(s), 1309(s), 1278(w), 1206(m), 1151(m), 1029(w), 961(m), 898(m), 790(s), 745(m), 663(w), 596(m), 541(w), 482(w).

X-ray crystal structure determination

The X–ray diffraction data taken at room temperature for complexes **Zn1** and **Cd1** were collected on a Rigaku R–AXIS RAPID IP diffractometer equipped with graphite–monochromated Mo Kα radiation (λ = 0.71073 Å). The structures of **Zn1** and **Cd1** were solved by direct methods and refined on F^2 by the full–matrix least squares using the SHELXTL–97 crystallographic software.[27,28] Anisotropic thermal parameters are refined to all of the non–hydrogen atoms. The hydrogen atoms were

held in calculated positions on carbon atoms and nitrogen atoms. The CCDC 1055702 and 1055703 contain the crystallographic data **Zn1** and **Cd1** of this paper. These data can be obtained free of charge at www.ccdc.cam.ac.uk/ deposit. Crystal structure data and details of the data collection and the structure refinement are listed as Table 1, selected bond lengths and bond angles of **Zn1** and **Cd1** are listed as Table S1.

Table 1 Crystal data and structure refinement parameters of complexes **Zn1** and **Cd1**.

Identification code	**Zn1**	**Cd1**
Empirical formula	$C_{20}H_{12}N_2O_4Zn$	$C_{20}H_{12}N_2O_4Cd$
Formula mass	409.71	456.73
Crystal system	Monoclinic	Monoclinic
Space group	$C2$/c	$C2$/c
a (Å)	28.967(6)	28.893(6)
b (Å)	8.053 (16)	8.239(16)
c (Å)	15.285(3)	15.421(3)
α (°)	90.00	90.00
β (°)	114.27(3)	113.10(3)
γ (°)	90.00	90.00
V (Å^3)	3250.4(11)	3376.5(12)
Z	8	8
D_c/(g · cm^{-3})	1.674	1.797
μ (Mo Kα)/mm^{-1}	1.542	1.324
$F(000)$	1664	1808
θ range (°)	3.09 – 27.47	3.07 – 27.48
	$-37 \le h \le 36$	$-33 \le h \le 37$
Limiting indices	$-10 \le k \le 10$	$-9 \le k \le 10$
	$-19 \le l \le 19$	$-19 \le l \le 20$
Data/Restraints/Parameters	3716 / 0 / 244	3866 / 0 / 244
GOF on F^2	1.022	1.194
Final R indices $[I > 2\sigma(I)]$		
$R_1{}^a$	0.0469	0.0305
$wR_2{}^b$	0.0966	0.0706
R indices (alldata)		
R_1	0.0782	0.0375
wR_2	0.1082	0.0735
CCDC	1055702	1055703

$^a R_1 = \sum ||F_o| - |F_c|| / \sum |F_o|$; $^b wR_2 = [\sum [w (F_o^2 - F_c^2)^2] / \sum [w (F_o^2)^2]]^{1/2}$.

Results and discussion

Structure description of [Zn(3-qlc)$_2$]$_n$ (Zn1) and [Cd(3-qlc)$_2$]$_n$ (Cd1)

The asymmetric unit consists of one Zn(II) or Cd(II) cation, two 3-qlc⁻ anions (Fig. 1a, b) for **Zn1** and **Cd1**. However, Zn(II) site takes the four-coordinated tetrahedral coordination geometry and the Cd(II) site takes the six-coordinated slightly distorted

octahedron coordination geometry (Fig. 1c, d). Comparison of Zn(II) to Cd(II), they both have d^{10} full-filled electron orbit, the difference is that Zn(II) has $3d^{10}$ as outer shell while Cd(II) has $4d^{10}$ as outer shell. Accordingly, the Cd(II) ionic radius is larger than that of Zn(II) which leads to form the covalent bonds in different bond strength, bond lengths and bond angles with the same organic ligands. As a consequence, even if the complexes formed by Cd(II) and Zn(II) have the same ligands and composition, they crystallize in the different structures. X-ray analysis reveals that the hexacoordinated Cd(II) cation is connected with four oxygen atoms and two nitrogen atoms from two individual 3-qlc⁻ anions to give a $[CdN_2O_4]$ coordination geometry. The central Zn(II) cation is tetracoordinated and forms a distorted tetrahedral geometry, completed by two oxygen atoms and two nitrogen atoms from two individual 3-qlc⁻ anions. Four oxygen atoms display the bidentate-chelate mode to connect center metal Cd(1). Two oxygen atoms adopt a monodentate fashion providing one sites to bond to center metal Zn(1). Nitrogen atoms from two quinoline rings display the η_N^1 mode to connect metal center Cd(1)/Zn(1). Among them, Cd–O bond lengths range from 2.164(2) Å to 2.765(2) Å, Cd(1)–N1 and Cd(1)–N2 bond lengths are 2.332(2) Å and 2.348(2) Å. O–Cd–O bond angles range from 56.1(7)° to 158.9(9)°, N–Cd–N bond angle is 97.3(8)°, O–Cd–N bond angles are in the range of 96.5(8)–152.6(9)°. Zn(1)–O1 and Zn(1)–O3 bond lengths are 1.968(3) Å and 1.927(2) Å, Zn(1)–N1 and Zn(1)–N2 bond lengths are 2.106(3) Å and 2.097(3) Å. O–Zn–O bond angle is 138.4(1)°, N–Zn–N bond angle is 100.9 (1)°, O–Zn–N bond angles are in the range of 100.3(1)–110.2(1)°. Zinc cations are connected through one 3-qlc⁻ anion giving rise to an infinite 1D chain (Fig. 1e, as an example of **Zn1**). Two adjacent 1D chains are combined by other 3-qlc⁻ anion forming 2D layer structure (Fig. 1f).
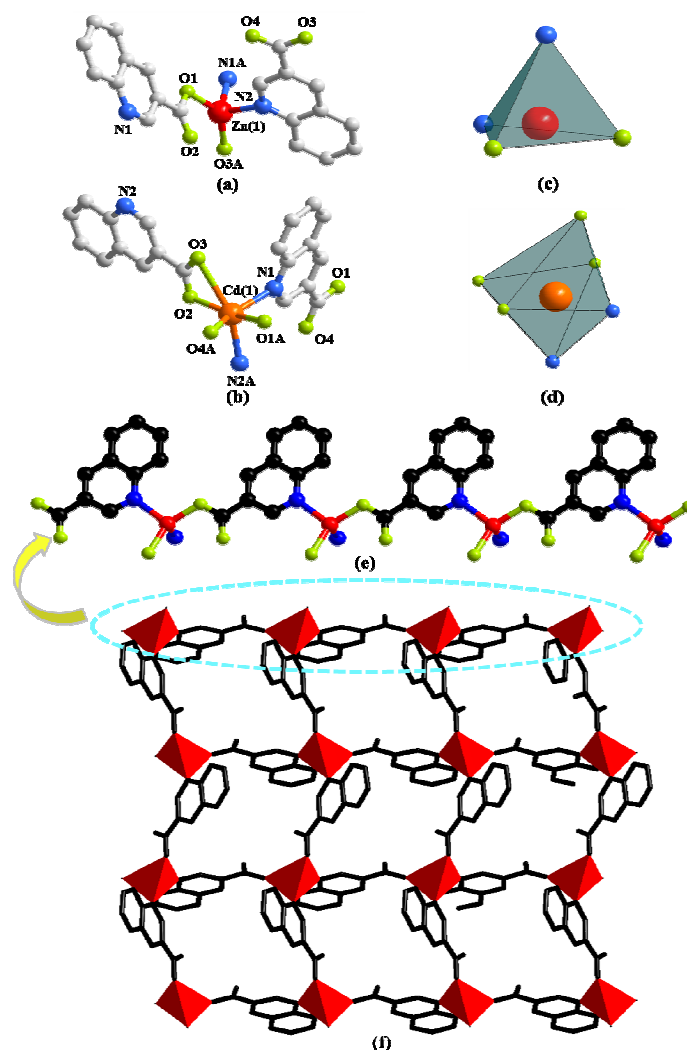
Fig. 1 The molecular structures of complex **Zn1** (a) and complex **Cd1** (b). All hydrogen atoms have been omitted for clarity. (c) Polyhedral representation of the coordination sphere of the Zn(1) centre in **Zn1**. (d) Polyhedral representation of the coordination sphere of the Cd(1) centre in **Cd1**. (e) Ball–and–stick representation of the 1D chain structure in **Zn1**. (f) The illustration of 2D layer structure in **Zn1**.

Moreover, inter-layer $\pi\cdots\pi$ stacking interaction with the distance of 3.479(2) Å and 3.506(1) Å between the centers of two quinoline rings, links the adjacent coordination layers to form a 3D network (Fig. 2a). Topological analysis has been applied for better understanding the connectivity of 3D framework in **Zn1**. When we consider the Zn(II) cation as the 6-connected node, the 3-qlc⁻ anions and two kinds of inter-layer $\pi\cdots\pi$ stacking interactions as the linkers, the simplified topological representation of **Zn1** can be described in Fig. 2b, which exhibits a 3D 6-connected primitive cubic (**pcu**) topological type with point symbol $(4^{12}.6^3)$ and vertex symbol (4.4.4.4.4.4.4.4.4.4.4.4.*.*.*).
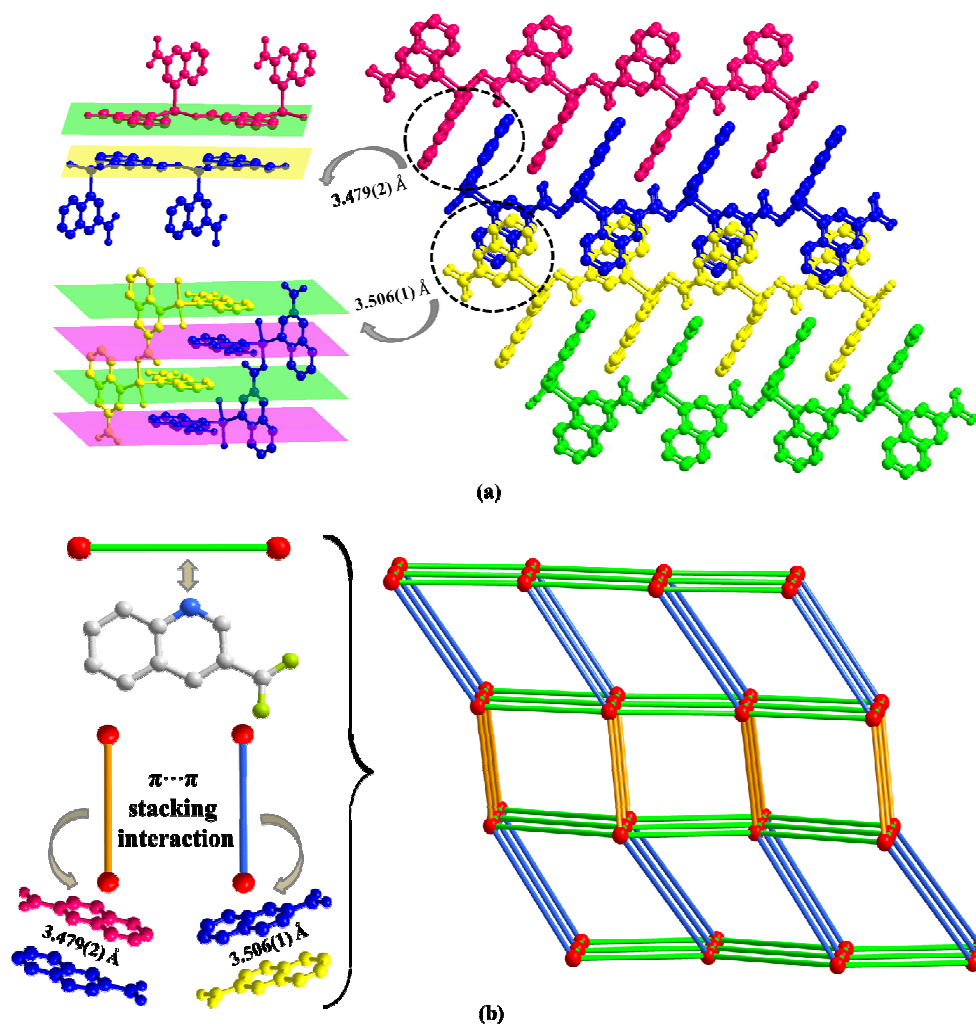
Fig. 2 (a) 3D supramolecular network constructed by inter-layer $\pi\cdots\pi$ interaction in **Zn1**. (b) The 3D **pcu** topology in its most symmetrical form distinguished by different colors (Color code: Zn(II) cation, red ball; 3-qlc⁻ anions, green line; inter-layer $\pi\cdots\pi$ stacking interaction with the distance of 3.479(2) Å, golden line; inter-layer $\pi\cdots\pi$ stacking interaction with the distance of 3.506(1) Å, blue line).

Thermal Gravimetric Analysis and Powder X-ray Diffraction Patterns

To characterize the complexes in terms of thermal stability, thermal gravimetric analysis (TGA) of **Zn1** and **Cd1** were carried out from room temperature to 700 °C under a flow of air (Fig. S2). **Zn1** shows the mass loss of 81.76% in the range 376–488 °C, corresponding to the release of two 3-Hqlc ligands (calcd 84.04%), and the main framework has collapse. The remaining residue of 18.24% is consistent with the formation of ZnO (calcd 19.86%). In **Cd1**, the weight loss of 72.81% from 369 °C to 461 °C corresponds to the loss of two 3-Hqlc ligands (calcd 75.39%), and the host framework has collapse. The remaining residue of 27.19% (calcd 28.12%) is

consistent with the formation of CdO.[29,30] Powder X-ray diffraction (PXRD) was used to check the purity of complexes **Zn1** and **Cd1** (Fig. S3). All the peaks displayed in the measured patterns are similar to those in the simulated patterns generated from single-crystal diffraction data, indicating single phases of **Zn1** and **Cd1** are formed. The differences in intensity may be owing to the preferred orientation of the powder samples.[31]

Luminescence properties

The d^{10} metal ions have drawn much attention in the construction of luminescent complexes not only for their variable surroundings but also for their changeable luminescent features by adopting different coordination modes, connection or interaction with functional ligands and the change of temperature.[32,33] The emission spectral data along with the lifetimes for complexes **Zn1** and **Cd1**, both in solution and in the solid state, are summarized in Tables S2. The luminescent spectra of **Zn1**, **Cd1** were measured at 298 K and 77 K in the solid state (Fig. 3a). The maximum emission band for **Zn1** is located at 468 nm (450 nm for **Cd1**), exhibiting blue luminescent emissions at 298 K. These luminescent emissions may be attributed to the ligand-centered $\pi^* \rightarrow \pi$ transition (Fig. S4).[34] The difference in luminescent details between **Zn1** and **Cd1** may be assigned to the different coordinating surroundings of the metal atoms and their distinct structure features. At 77 K, **Zn1** has higher-energy emission of one shoulder-peaks appearing around 483^{sh}. The maximum emission band for **Zn1** is located at 510 nm and the lower-energy emission bond centered at 571^{sh} nm (449^{sh}, 485, 542^{sh} nm for **Cd1**), which are in the green region. The luminescence quantum yields (Φ) of complexes **Zn1** and **Cd1** were determined by means of an integrating sphere at 298 K and 77 K under the excitation wavelengths. The solid state measurements gave luminescence quantum yields of 11.68% for **Zn1** and 11.03% for **Cd1** at 298 K. The corresponding Φ value of **Cd1** is smaller than that of **Zn1**, because of the heavy-atom effect. When measurement temperature is reduced to 77 K, the quantum yield mounts up to 16.46% for **Zn1** and 15.71% for **Cd1**. Meanwhile, the lifetimes of **Zn1** and **Cd1** increase conspicuously compared to those at 298 K (298 K: τ= 7.76 μs for **Zn1**, τ= 7.50 μs for **Cd1**; 77 K: τ= 10.76 μs for **Zn1**, τ= 9.91 μs for **Cd1**) (Fig. 3b). This is most likely due to the fact that cold conditions should be favorable for the rigidity of ligands with reducing the non-radiation decay and collisional quenching. Thereby the increase of quantum yields and the lifetimes could be observed eventually at lowering the temperature.[35,36]
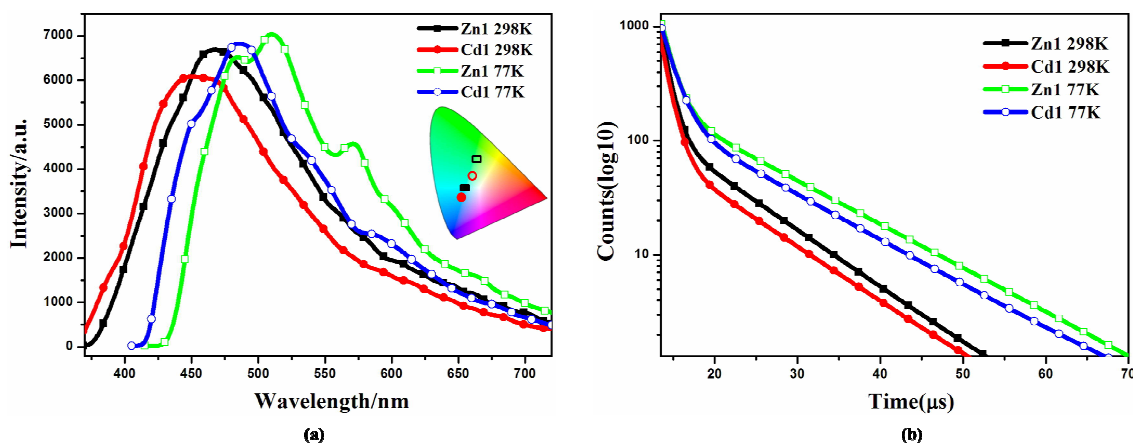
Fig. 3 (a) Emission spectra of complexes **Zn1** and **Cd1** at 298 K, 77 K in solid state and the corresponding color coordinate diagram of emission. (b) The decay curves of complexes **Zn1** and **Cd1** at 298 K and 77 K in solid state.

The obtained **Zn1** and **Cd1** readily dissolve in common organic solvents, such as dimethyl sulfoxide (DMSO), methanol (CH$_3$OH), chloroform (CHCl$_3$) and tetrahydrofuran (THF). The maximum emission wavelengths of the **Zn1** and **Cd1** are red-shifted by ~10 nm (409 nm in THF, 412 nm in CHCl$_3$ and 418 nm in CH$_3$OH for **Zn1**; 405 nm in THF, 407 nm in CHCl$_3$ and 412 nm in CH$_3$OH for **Cd1**) in the corresponding solvents, and all the studied moieties generated blue emission with CIE coordinates of 0.18, 0.14–0.20, 0.21 (Fig. 4). As solvent polarity increases (polarity: THF < CHCl$_3$ < CH$_3$OH < DMSO), the emission intensity of the complexes gradually diminishes. In particular, the emission spectrum of **Zn1** and **Cd1** becomes broader and weaker in the DMSO solvent (424 nm and 418 nm), with CIE coordinates of 0.19, 0.20 and 0.19, 0.16.
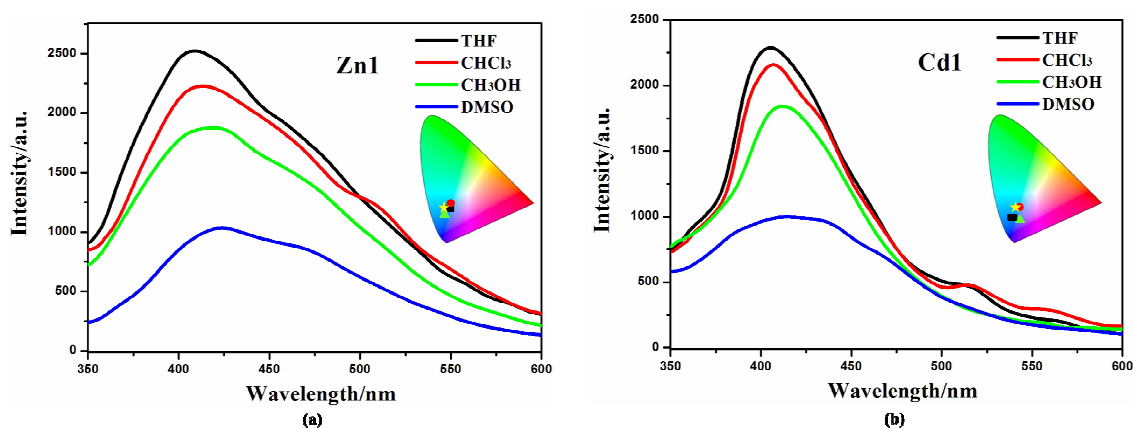
Fig. 4 Emission spectra of **Zn1** (a) and **Cd1** (b) in different solvents (excited at 330 nm) and the corresponding color coordinate diagram of emission (rectangle: THF; roundness: CHCl$_3$; triangle CH$_3$OH; pentacle: DMSO).

In addition, **Zn1** and **Cd1** are insoluble in water (H_2O). The aggregated particles should be precipitated as the fraction of water is increased. The emission spectra of **Zn1** and **Cd1** in DMSO/water mixtures with different water content (0−99%) were obtained to verify if the **Zn1** and **Cd1** displayed AIE properties. This is done by adding different amount of water to the pure DMSO solutions to obtain water fraction (f_w) of 0-99% and monitored the changes of luminescence. The concentration was maintained at 10^{-5} M. At every increment of water fraction (f_w), the emission spectrum is collected. All f values are volume/volume percentages. As shown in Fig. 5, there is a clear trend that **Zn1** and **Cd1** are weak emissive in DMSO solution, but when they aggregates due to the addition of water, as a poor solvent, the emission dramatically increase after a large amount of water have been added. The luminescence enhancement from the solution state to the aggregated state is defined by the AIE factor (α_{AIE}): $\alpha_{AIE,I} = I_{aggr}/I_{soln}$, where I_{aggr} and I_{soln} are the luminescence intensity of the aggregates and solution, respectively. The luminescence intensity of **Zn1** and **Cd1** in the DMSO/water mixture with 99 vol% H_2O is 6.06-fold and 5.43-fold higher than that in DMSO solution, respectively.[37] This is most likely due to the fact, when the molecules are aggregated; such free rotations are hindered because of the short distances among the crowded molecules. Thus, the nonradiative energy consuming pathway is blocked and strong emission is vitalized. For **Zn1** and **Cd1**: the building blocks of the crystals are not the monomers, but rather the dimers, based on the intermolecular π⋯π stacking interactions between adjacent carboxylic acid groups and quinoline rings, this structure further increases the rigidity of the molecules to generate a more extended planar skeleton, which restricts the intermolecular rotations, and may extend the conjugation system by incorporating the carboxylate oxygen and nitrogen atoms to the 3-Hqlc ligand, and thus might influence the luminescent. **Zn1** and **Cd1** as new AIE materials show advantages of high sensitivity, and may shed light on the development of new probes for luminescent applications.[38]
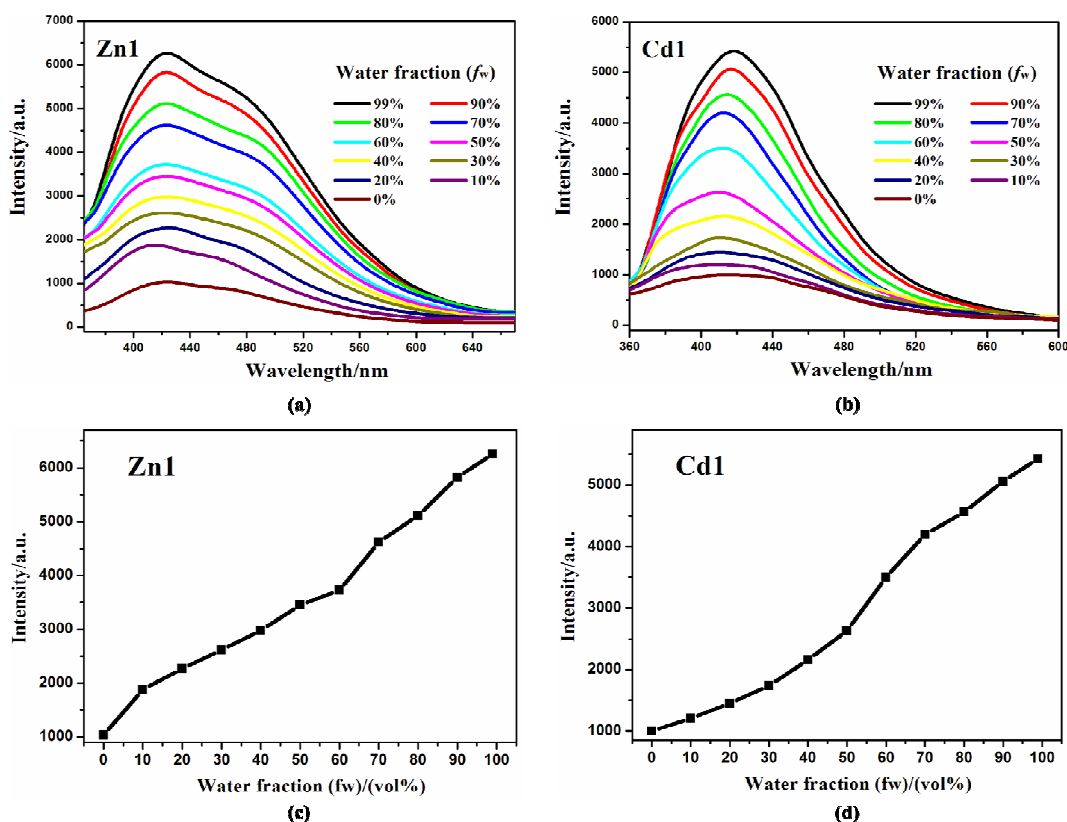
Fig. 5 Emission spectra of **Zn1** (a) and **Cd1** (b) in DMSO/water mixtures with different water fractions (f_w) at 298 K under excitation at 330 nm. (c) The changes in the luminescence peak intensity with different water fractions of **Zn1**. (d) The changes in the luminescence peak intensity with different water fractions of **Cd1**.

Application in DSSCs

The UV-visible absorption spectra of **Zn1**, **Cd1** and N719 in ethanol solution are displayed in Fig. 6, and the corresponding data are listed in Table 2. Two main absorption bands for **Zn1** and **Cd1** can be observed. The two prepared complexes display weak absorption bands at around 325 nm with strong absorption peaks at ca. 386 nm. Encouraged by the UV-visible absorption result, **Zn1** and **Cd1** can be considered as co-sensitizers used in N719 sensitized DSSCs. The molar extinction coefficients in the blue-violet region are 51,079 M^{-1} cm^{-1} for **Zn1** and 48,693 M^{-1} cm^{-1} for **Cd1**. All of these are much higher than that of the ruthenium complex N719.[39] A higher molar extinction coefficient indicates that the **Zn1** or **Cd1** possesses a higher light harvesting ability in this wavelength region compared with N719 and I_3^- (25,000M^{-1} cm^{-1}).[40] Hence it can be predicted that the photon lost due to the light absorption by I_3^- will be suppressed by the use of **Zn1** or **Cd1** as a co-sensitizer due to the competition between **Zn1** or **Cd1** and I_3^- to absorb light.
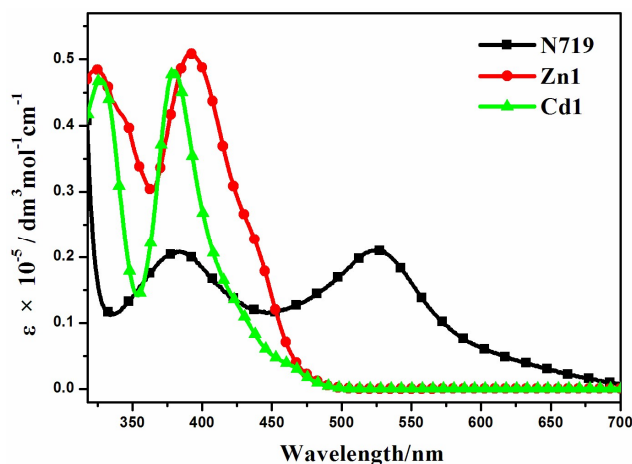
Fig. 6 UV-visible absorption spectra of **Zn1**, **Cd1** and N719 in ethanol.

Energy matching is crucial in selecting sensitizers for DSSCs. Therefore, in order to evaluate if there are favorable energy offsets of the prepared complexes with respect to the TiO$_2$ film and the electrolyte, the HOMO and LUMO energy levels of **Zn1** and **Cd1** were investigated by cyclic voltammetry (CV) measurement in a three-electrode cell and an electrochemistry workstation. The experimental data are summarized in Table 2. As estimated from the intersection of the absorption and emission spectra, the excitation transition energy (E$_{0-0}$) of **Zn1** and **Cd1** are 3.11 and 3.17 eV, respectively. Consequently, the HOMO values of **Zn1** and **Cd1** are calculated based on their first redox potentials as -5.24 and -5.33 eV, respectively, and the LUMO levels of **Zn1** and **Cd1** calculated from E$_{HOMO}$ + E$_{0-0}$, are -2.13 and -2.16 eV, respectively.[41] The HOMO and LUMO energy levels of **Zn1** and **Cd1** are shown in Scheme 1. It shows that the energy levels of the prepared complexes are appropriate for the DSSCs system containing TiO$_2$. The LUMO levels lied above the conduction band of the TiO$_2$ semiconductor (-4.40 eV vs vacuum), indicating efficient electron injection, and the HOMO energy levels lied below the I$^-$/I$_3$ redox electrolyte (-4.60 eV *vs* vacuum) which is further improved negatively about 0.3 V by adding additives such as 4-*tert*-butyl pyridine (TBP) to the I$^-$/I$_3^-$ redox electrolyte, providing sufficient driving force for dye regeneration.[42]

Table 2 Experimental data for spectral and electrochemical properties of the complexes **Zn1** and **Cd1**.

Dyes	λ$_{abs}$(nm)[a]	ε(M^{-1}cm^{-1})[a]	λ$_{em}$(nm)[a,b]	E$_{0-0}$(eV)[c]	E$_{ox}$/V vs SCE[d]	E$_{HOMO}$(eV)[e]	E$_{LUMO}$(eV)[e]
Zn1	392	51079	409	3.11	0.84	-5.24	-2.13
Cd1	380	48693	406	3.17	0.93	-5.33	-2.16

[a] Absorption and emission spectra were recorded in ethanol solution (10^{-5} M) at room temperature.

[b] Complexes were excited at their absorption maximum value

[c] Optical band gap calculated from intersection between the absorption and emission spectra.

[d] The first oxidation potentials of complexes were obtained by CV measurement.

[e] The values of E_{HOMO} and E_{LUMO} were calculated with the following formula:

$HOMO\,(eV) = -e(E_{onset}^{ox}\,V + 4.4V); \quad LUMO\,(eV) = E_{HOMO} + E_{0-0}$

where E_{0-0} is the intersection of absorption and emission of the complexes **Zn1** and **Cd1**.
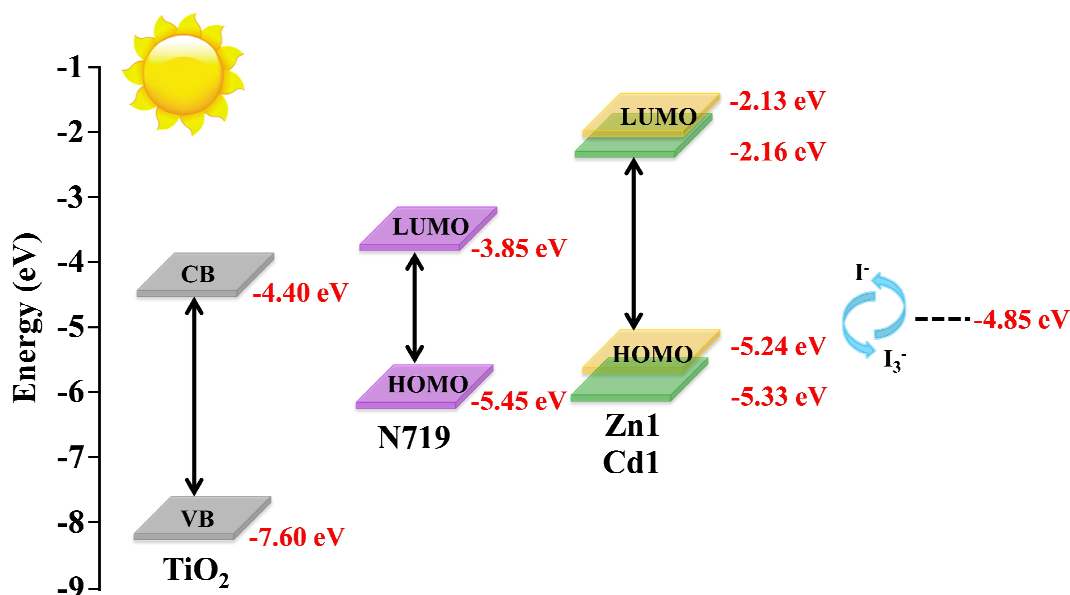
Scheme 1 Schematic energy diagram of HOMO and LUMO for dyes compared to the energy levels calculated for TiO$_2$.

Fig. 7 presents the performances of the co-sensitized DSSCs in terms of J_{sc} and V_{oc}, and the results of all DSSCs are list in Table 3. The result indicates that the photochemical performance of co-sensitized photoelectrodes has been enhanced. The present work indicated that d^{10} metal coordination complexes could affect the photochemical performance of DSSCs due to proton number. Fig. 7a and Table 3 indicate that the performances of cells co-sensitized with **Zn1** or **Cd1** and N719 are improved in the order of **Zn1**/N719 > **Cd1**/N719 > N719. As shows in Table 3, the co-sensitized solar cell based on a **Zn1**/N719/TiO$_2$ and **Cd1**/N719/TiO$_2$ electrode yield a remarkably high photocurrent density (J_{sc}) of 18.61 mA cm^{-2} and 18.36 mA cm^{-2} under standard global AM 1.5 solar irradiation conditions without an expense of lower open circuit voltage (V_{oc}) but a little increased from 0.73 V to 0.72 V. The cell shows a better photo-electricity conversion efficiency of 7.75% and 7.70%, which is higher than that for DSSCs using single N719 (5.36%). In this way the cell efficiency was improved by more than 44.59% and 43.66% compared with that for single N719.

This result suggests that co-sensitization of TiO$_2$ photoelectrode with the **Zn1** or **Cd1** and N719 is an effective way to improve the efficiency of DSSCs.

Table 3 *J-V* performance of DSSCs based on different photoelectrodes.

Photoelectrode	J_{sc}/mA/cm^2	V_{oc}/V	*FF*	η/%
N719/TiO$_2$	13.42	0.66	0.60	5.36
Zn1/N719/TiO$_2$	18.61	0.73	0.57	7.75
Cd1/N719/TiO$_2$	18.36	0.72	0.58	7.70

Dark-current measurement of DSSCs has been considered as a qualitative technique to describe the extent of the back electron transfer. A comparison of dark current between the investigated cells can provide useful information regarding the back electron transfer process. Fig. 7b shows the dark current–voltage characteristics of the DSSCs based on different photoelectrodes with the applied bias from 0 to +0.80 V. The onset of the dark current for individual N719-sensitized DSSC occurs at a bias of about +0.48 V, with a subsequent dramatic increase of dark current with the increase of potential. In contrast, for the co-sensitized DSSCs, the onset potential shifted to about +0.54 V for **Zn1**/N719 and **Cd1**/N719; furthermore, the dark current of the co-sensitized DSSCs increased much more slowly than that of N719-sensitized DSSC when the potential was greater than +0.54 V. Under the same potential bias, when the potential was ≥0.48 V, the dark current for the co-sensitized DSSCs was smaller than that for the N719-sensitized DSSC. The increase of the onset potential and the reduction of the dark current indicated that **Zn1** and **Cd1** successfully suppress the electron back reaction with I$_3^-$ in the electrolyte.
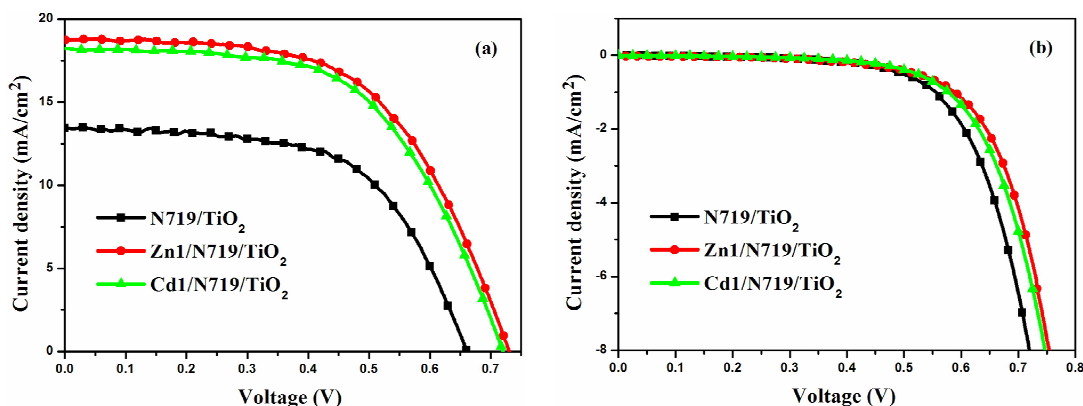
Fig. 7 *J–V* curves for DSSCs based on co–sensitized photoelectrodes and N719 sensitized photoelectrode under irradiation (a) and in dark (b).

The higher η value of co-sensitized solar cell compared with the individually N719 sensitized devices, is attributed to the enhanced photovoltaic parameters J_{sc} and V_{oc}. Particularly, the enhanced J_{sc} value is ascribed to the enhanced IPCE response of the cell, since they are related by the equation:

$$J_{sc} = \int e\phi_{ph.AM1.5G}(\lambda)d\lambda$$

where e is the elementary charge and $\phi_{ph.AM1.5G}$ is the photon flux at AM 1.5.[43-45] The IPCE spectra of different devices were collected in Fig. 8. The DSSCs containing only N719 dye has a broad IPCE spectrum from 400-750 nm, which is due to the competitive light absorption between I_3^- and N719. When the prepared complex is used as co-sensitizer, not only this decrease is restored, but also the IPCE spectrum in the whole visible region is enhanced. This is attributed to the fact that the prepared complexes have attached to the TiO_2 surface effectively and contributed to the electron injection into the conduction band of the TiO_2. This means the co-sensitization of N719 and prepared complex has a significant synergy and compensatory effect on light harvesting, electron injection and collection on TiO_2. Based on the IPCE and the absorption spectra, the cell's higher J_{sc} in the case of co-sensitization is mainly ascribed to better light harvesting in the low wavelength region, where the absorption of N719 is compensated and the competitive light absorption of I_3^- is overcome. Beside this, its enhanced spectra response in the whole visible region is also a main factor to improve J_{sc}.
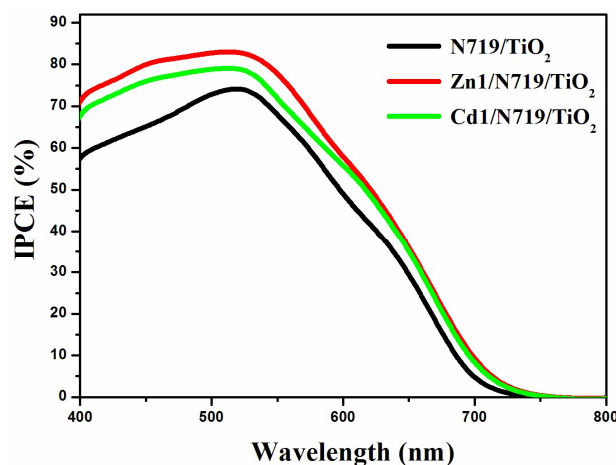
Fig. 8 The incident photon-to-current conversion efficiency spectra of devices based on single N719 sensitized and co-sensitized photoanodes.

The electrochemical impedance spectroscopy (EIS) is a steady-state method for examining the interfacial resistances and electron transport properties within an

electrochemical system.[46] The EIS investigation of the DSSC device provides valuable information for the understanding of photovoltaic parameters (J_{sc}, V_{oc}, FF, and η). Herein, we utilize EIS to analyze charge carrier dynamics in the interfacial regions of solid-liquid layers. Impedance spectra of DSSC devices with **Zn1**/N719 and **Cd1**/N719 co-sensitized photoanode were measured under standard global AM1.5 solar irradiation or in the dark by applying a forward bias equivalent to open circuit potential.[47] As indicated in Fig. 9, a typical EIS spectrum exhibits three semicircles in the Nyquist plot. In the order of increasing frequency the features are attributed to the Nernst diffusion in the electrolyte, electron transfer at the TiO_2/electrolyte interface, and redox charge transfer at the counter electrode, respectively.[48]

     Under light illumination, the second semicircle radius in the Nyquist plot decreased after co-sensitized with **Zn1** or **Cd1**, and the values are in the order of **Zn1**/N719 < **Cd1**/N719 < N719, which indicates a decrease of the electron transfer impedance and an increase of charge transfer rate at this interface (Fig. 9a); while in the dark, this semicircle radius in the Nyquist plot increased after co-sensitized with **Zn1** or **Cd1**, and the values are in the order of **Zn1**/N719 > **Cd1**/N719 > N719, which indicates an increase of electron recombination impedence and a reduction of the interfacial charge recombination rate (Fig. 9b).
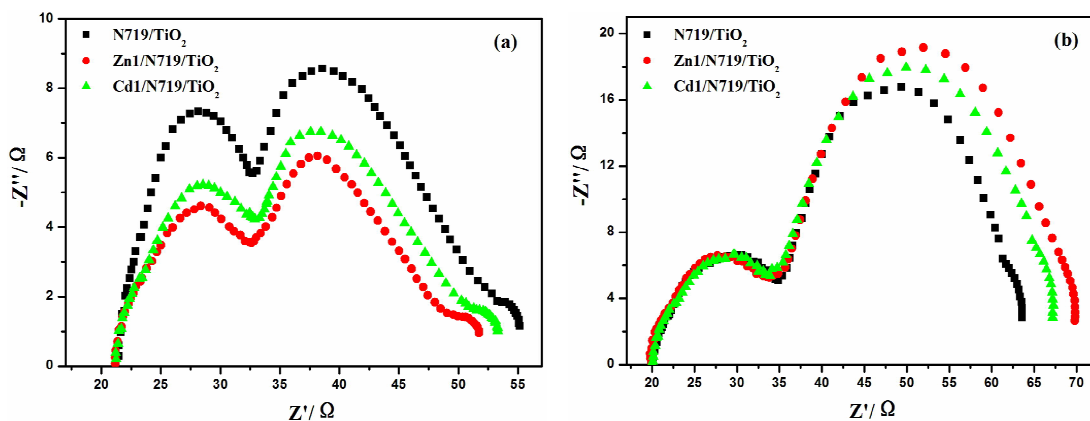
Fig. 9 Nyquist plots of EIS for DSSCs based on different photoelectrodes measured under standard AM1.5 G solar irradiation (a) and in dark (b) at forward bias –0.75V.

     In an effort to understand the enhancement of the V_{oc} value in the dye-sensitized solar cells, the electron lifetime (τ_e) in different devices were calculated by fitting the Bode plots of the EIS spectra of different solar cells in dark (Fig. 10), according to the relationship: $\tau_e = 1/(2\pi f_{max})$, where f_{max} is the frequency at the maximum of the curve in the intermediate frequency region in Bode phase plot.[49] The electron lifetimes (τ_e)

for the devices co-sensitized with prepared complexes (16.42 ms for **Zn1** and 15.77 ms for **Cd1**) were found to be longer than individually N719 sensitized device (8.59 ms). This difference might be expected, since the adsorption of prepared complexes may form a better dye coverage to help to passivate the TiO_2 surface or form an insulating molecular layer composed of prepared complexes and N719 molecules. It will reduce the recombination due to electron back-transfer between TiO_2 and I_3^-. This retardation of the charge recombination between injected electron and I_3^- ions in the electrolyte, leads to a consequent increase of V_{oc}. This appears to be consistent with the larger V_{oc} values sequence which is in the order of **Zn1**/N719 > **Cd1**/N719 > N719.
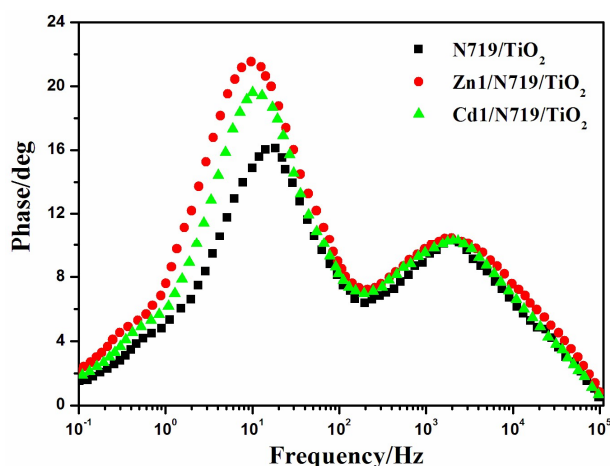
Fig. 10 Bode plots of EIS for DSSCs based on different photoelectrodes measured in dark conditions.

When the geometric and electronic structures of the complexes are taken into account, it is found that there is a relationship between crystal structure and DSSCs performance. For complexes **Zn1** and **Cd1**, they adsorbed on Nano TiO_2 thin film surface through carboxyl which have various coordination modes with metal ions. Although carboxyl has coordinated to the Cd^{2+}/Zn^{2+} ion, Ti^{4+} ion may also be coordinated with carboxyl due to the existence of lone pair electrons in carboxylate oxygen atom which could combine with Ti^{4+} ion to form Ti-O coordination bond, and further adsorbed on the TiO_2 film. Furthermore, the complexes **Zn1** and **Cd1** extend as 3D networks through π–π stacking interactions, which make the electron-donating ability of **Zn1** and **Cd1** better when they are used in DSSCs as co-sensitizers. All of these structural features of **Zn1** and **Cd1** result in obtaining higher performance of co-sensitized cells than that of cells sensitized by single N719. Meanwhile, for **Cd1**, the larger atom radius of Cd likely increases the Cd-O and Cd–N average bond

lengths, which are 2.403 Å and 2.340 Å (the average Zn-O and Zn–N bond lengths are 1.948 Å and 2.102 Å), indicating that Zn-O and Zn-N bond are more stable than Cd-O and Cd-N bond (Table S1). Apparently, the increased distance is not good for electron transfer. Therefore, the performance of the co-sensitized cell is in the order of **Zn1**/N719 > **Cd1**/N719.

Conclusion

Two new 2D d^{10} metal complexes with rigid 3-Hqlc ligand have been prepared and structurally characterized. The crystallographic data of **Zn1** and **Cd1** demonstrate that the formation of π···π stacking interactions can act as primary tool for constructing fascinating 3D network architectures. Complexes **Zn1** and **Cd1** show tunable luminescence (from blue to green) and photovoltaic properties. Both of them can display obvious AIE properties when they are dissolved in DMSO/water mixtures. The results reveal the potential of molecular design in functional luminescent complexes. Beyond that, we systematically investigated **Zn1** and **Cd1** as co-sensitizers in a ruthenium dye N719 based solar cell. The co-sensitization could enhance the spectral response of the N719 dye sensitized TiO$_2$ film, suppress the electron recombination and decrease the total resistance of DSSCs. The improvement in efficiency is attributed to the fact that **Zn1** and **Cd1** overcome the deficiency of N719 absorption in the region of ultraviolet and blue-violet. We believe that such complexes will further facilitate the exploration of new type of multifunctional material with interesting properties, including the combination of luminescence and dye-sensitized solar cells.

Acknowledgments

References

1 H. K. Chae, J. Kim, O. D. Friedrichs, M. O'Keeffe and O. M. Yaghi, *Angew. Chem. Int. Ed.*, 2003, **42**, 3907–3909.

2 J. Seo, C. Bonneau, R. Matsuda, M. Takata and S. Kitagawa, *J. Am. Chem. Soc.*,

2011, **133**, 9005–9013.

3 Z. H. Yan, W. Wang, L. L. Zhang, X. W. Zhang, L. Wang, R. M. Wang and D. F. Sun, *RSC Adv.*, 2015, **5**, 16190–16198.

4 Z. C. Hu, B. J. Deibert and J. Li, *Chem. Soc. Rev.*, 2014, **43**, 5815–5840.

5 R. R. Hu, N. L. C. Leung and B. Z. Tang, *Chem. Soc. Rev.*, 2014, **43**, 4494–4562.

6 Y. X. Guo, X. Feng, T. Y. Han, S. Wang, Z. G. Lin, Y. P. Dong and B. Wang, *J. Am. Chem. Soc.*, 2014, **136**, 15485–15488.

7 X. Y. Huang, S. Y. Han, W. Huang and X. G. Liu, *Chem. Soc. Rev.*, 2013, **42**, 173–201.

8 J. Z. Zhang, J. Zhang, H. B. Li, Y. Wu, H. L. Xu, M. Zhang, Y. Geng and Z. M. Su, *J. Power Sources*, 2014, **267**, 300–308.

9 G. De Filpo, F. P. Nicoletta, L. Ciliberti, P. Formoso and G. Chidichimo, *J. Power Sources*, 2015, **274**, 274–279.

10 D. D. Wang, Y. Wu, H. Dong, Z. X. Qin, D. Zhao, Y. Yu, G. J. Zhou, B. Jiao, Z. X. Wu, M. Gao and G. Wang, *Org. Electron.*, 2013, **14**, 3297–3305.

11 L. G. Wei, Y. L. Yang, R. Q. Fan, Y. Na, P. Wang, Y. W. Dong, B. Yang and W. W. Cao, *Dalton Trans.*, 2014, **43**, 11361–11370.

12 G. D. Sharma, D. Daphnomili, K. S. V. Gupta, T. Gayathri, S. P. Singh, P. A. Angaridis, T. N. Kitsopoulos, D. Tasis and A. G. Coutsolelos, *RSC Adv.*, 2013, **3**, 22412–22420.

13 X. Wang, Y. L. Yang, P. Wang, L. Li, R. Q. Fan, W. W. Cao, B. Yang, H. Wang and J. Y. Liu, *Dalton Trans.*, 2012, **41**, 10619–10625.

14 X. X. Li, H. Y. Xu, F. Z. Kong and R. H. Wang, *Angew. Chem. Int. Ed.*, 2013, **52**, 13769–13773.

15 A. Schneemann, V. Bon, I. Schwedler, I. Senkovska, S. Kaskel and R. A. Fischer, *Chem. Soc. Rev.*, 2014, **43**, 6062–6096.

16 F. A. Almeida Paz, J. Klinowski, S. M. F. Vilela, J. P. C. Tomé, J. A. S. Cavaleiro and J. Rocha, *Chem. Soc. Rev.*, 2012, **41**, 1088–1110.

17 A. Báez-Castro, J. Baldenebro-López, A. Cruz-Enríquez, H. Höpfl, D. Glossman-Mitnik, M.-S. Valentín, M. Parra-Hake and J. J. Campos-Gaxiola, *RSC Adv.*, 2014, **4**, 42624–42631.

18 C. B. Liu, Q. Li, X. Wang, G. B. Che and X. J. Zhang, *Inorg. Chem. Commun.*, 2014, **39**, 56–60.

19 Y. Gong, M. M. Zhang, J. B. Qin, J. Li, J. P. Meng and J. H. Lin, *Dalton Trans.*,

2014, **43**, 8454–8460.

20 L. Croitor, E. B. Coropceanu, A. E. Masunov, H. J. Rivera-Jacquez, A. V. Siminel and M. S. Fonari, *J. Phys. Chem. C*, 2014, **118**, 9217–9227.

21 L. Croitor, E. B. Coropceanu, A. E. Masunov, H. J. Rivera-Jacquez, A. V. Siminel, V. I. Zelentsov, T. Y. Datsko and M. S. Fonari, *Cryst. Growth Des.*, 2014, **14**, 3935−3948.

22 S. Altobello, R. Argazzi, S. Caramori, C. Contado, S. Da Fré, P. Rubino, C. Choné, G. Larramona and C. A. Bignozzi, *J. Am. Chem. Soc.*, 2005, **127**, 15342–15343.

23 S. Archer and J. A. Weinstein, *Coord. Chem. Rev.*, 2012, **256**, 2530–2561.

24 T. Swetha, S. Niveditha, K. Bhanuprakash and S. P. Singh, *Electrochim. Acta*, 2015, **153**, 343–351.

25 Y. Z. Xie, G. G. Shan, P. Li, Z. Y. Zhou and Z. M. Su, *Dyes Pigm.*, 2013, **96**, 467–474.

26 L. Chen, Y. B. Jiang, H. Nie, R. R. Hu, H. S. Kwok, F. Huang, A. J. Qin, Z. J. Zhao and B. Z. Tang, *ACS Appl. Mater. Interfaces*, 2014, **6**, 17215–17225.

27 G. M. Sheldrick, S$_{HELXL}$ 97 Program for Crystal Structure Refinement; University of GÖttingen, GÖttingen, Germany, 1997.

28 G. M. Sheldrick, S$_{HELXL}$ 97 Program for Crystal Structure Solution; University of GÖttingen, GÖttingen, Germany, 1997.

29 D. M. Chen, X. P. Zhang, W. Shi and P. Cheng, *Cryst. Growth Des.*, 2014, **14**, 6261−6268.

30 L. M. Fan, W. L. Fan, B. Li, X. Z. Liu, X. Zhao and X. T. Zhang, *RSC Adv.*, 2015, **5**, 14897–14905.

31 J. Yang, J. F. Ma, Y. Y. Liu and S. R. Batten, *CrystEngComm*, 2009, **11**, 151–159.

32 Y. Kim, J. H. Song, W. R. Lee, W. J. Phang, K. S. Lim and C. S. Hong, *Cryst. Growth Des.*, 2014, **14**, 1933−1937.

33 P. Chakraborty, J. Adhikary, S. Samanta, D. Escudero, A. C. Castro, M. Swart, S. Ghosh, A. Bauzá, A. Frontera, E. Zangrando and D. Das, *Cryst. Growth Des.*, 2014, **14**, 4111−4123.

34 R. Q. Fan, Y. L. Yang, Y. B. Yin, W. Hasi and Y. Mu, *Inorg. Chem.*, 2009, **48**, 6034–6043.

35 R. R. Hu, C. F. A. Gómez-Durán, J. W. Y. Lam, J. L. Belmonte-Vázquez, C. M. Deng, S. J. Chen, R. Q. Ye, E. Peña-Cabrera, Y. C. Zhong, K. S. Wong and B. Z. Tang, *Chem. Commun.*, 2012, **48**, 10099–10101.

36 Q. L. Zhu, C. J. Shen, C. H. Tan, T. L. Sheng, S. M. Hu and X. T. Wu, *Chem. Commun.*, 2012, **48**, 531–533.

37 P. Y. Gu, C. J. Lu, Z. J. Hu, N. J. Li, T. T. Zhao, Q. F. Xu, Q. H. Xu, J. D. Zhang and J. M. Lu, *J. Mater. Chem. C*, 2013, **1**, 2599–2606.

38 M. Zhang, G. X. Feng, Z. G. Song, Y. P. Zhou, H. Y. Chao, D. Q. Yuan, T. T. Y. Tan, Z. G. Guo, Z. G. Hu, B. Z. Tang, B. Liu and D. Zhao, *J. Am. Chem. Soc.*, 2014, **136**, 7241–7244.

39 D. B. Kuang, S. Ito, B. Wenger, C. Klein, J. E. Moser, R. Humphry-Baker, S. M. Zakeeruddin and M. Grätzel, *J. Am. Chem. Soc.*, 2006, **128**, 4146–4154.

40 G. D. Sharma, S. P. Singh, R. Kurchania and R. J. Ball, *RSC Adv.*, 2013, **3**, 6036–6043.

41 L. G. Wei, Y. Na, Y. L. Yang, R. Q. Fan, P. Wang and L. Li, *Phys. Chem. Chem. Phys.*, 2015, **17**, 1273–1280.

42 K. R. Justin Thomas, Y. C. Hsu, J. T. Lin, K. M. Lee, K. C. Ho, C. H. Lai, Y. M. Cheng and P. T. Chou, *Chem. Mater.*, 2008, **20**, 1830–1840.

43 J. A. Mikroyannidis, M. S. Roy and G. D. Sharma, *J. Power Sources*, 2010, **195**, 5391–5398.

44 G. H. Wu, F. T. Kong, J. Z. Li, X. Q. Fang, Y. Li, S. Y. Dai, Q. Q. Chen and X. X. Zhang, *J. Power Sources*, 2013, **243**, 131–137.

45 J. Cui, J. F. Lu, X. B. Xu, K. Cao, Z. Wang, G. Alemu, H. L. Yuang, Y. Shen, J. Xu, Y. B. Cheng and M. K. Wang, *J. Phys. Chem. C*, 2014, **118**, 16433−16440.

46 F. Malara, A. Cannavale, S. Carallo and G. Gigli, *ACS Appl. Mater. Interfaces*, 2014, **6**, 9290–9297.

47 J. Bisquert, A. Zaban, M. Greenshtein and I. Mora-Sero, *J. Am. Chem. Soc.*, 2004, **126**, 13550–13559.

48 D. B. Kuang, S. Uchida, R. Humphry-Baker, S. M. Zakeeruddin and M. Grätzel, *Angew. Chem. Int. Ed.*, 2008, **47**, 1923–1927.

49 S. P. Singh, K. S. V. Gupta, M. Chandrasekharam, A. Islam, L. Y. Han, S. Yoshikawa, M. Haga, M. S. Roy and G. D. Sharma, *ACS Appl. Mater. Interfaces*, 2013, **5**, 11623–11630.

Table of Contents

Multifunctional Zn(II)/Cd(II) Metal Complexes for Tunable Luminescence Properties and High Efficient Dye-Sensitized Solar Cells

Song Gao,[a] Rui Qing Fan,*[a] Xin Ming Wang,[a] Liang Sheng Qiang,[a] Li Guo Wei,[a] Ping Wang,[a] Yu Lin Yang,*[a] Yu Lei Wang,[b] Tian Zhu Luan[c]

[a] *Department of Chemistry, Harbin Institute of Technology, Harbin 150001, P. R. China*

[b] *National Key Laboratory of Science and Technology on Tunable Laser, Harbin Institute of Technology, Harbin 150080, P. R. China*

[c] *The First Affiliated Hospital of Harbin Medical University, Harbin, 150001, P. R. China*

Complexes **Zn1** and **Cd1** exhibit tunable luminescence properties and they can serve as co-sensitizer to enhance the power-conversion efficiency.